

Optical characterization and lasing in three-dimensional opal-structures

Yoshiaki Nishijima^{1*} and Saulius Juodkazis^{2,3,4*}

¹ Department of Electrical and Computer Engineering, Graduate School of Engineering, Yokohama National University, Yokohama, Japan, ² Centre for Micro-Photonics, Faculty of Science, Engineering and Technology, Swinburne University of Technology, Melbourne, VIC, Australia, ³ Melbourne Centre for Nanofabrication (MCN), Australian National Fabrication Facility, Clayton, VIC, Australia, ⁴ Center of Nanotechnology, King Abdulaziz University, Jeddah, Saudi Arabia

OPEN ACCESS

Edited by:

P. Davide Cozzoli,
University of Salento, Italy

Reviewed by:

Carola Kryschi,
Friedrich-Alexander Universität
Erlangen-Nürnberg, Germany
Francesco Scotognella,
Politecnico di Milano, Italy

*Correspondence:

Yoshiaki Nishijima,
Department of Electrical and
Computer Engineering, Graduate
School of Engineering, Yokohama
National University, 79-5
Tokiwadai, Hodogaya-ku, Yokohama
240-8501, Japan
nishijima@ynu.ac.jp;
Saulius Juodkazis,
Centre for Micro-Photonics, Faculty of
Science, Engineering and Technology,
Swinburne University of Technology,
3122 Hawthorn, VIC, Australia
sjuodkazis@swin.edu.au

Specialty section:

This article was submitted to *Colloidal Materials and Interfaces*, a section of the journal *Frontiers in Materials*

Received: 26 January 2015

Accepted: 03 June 2015

Published: 19 June 2015

Citation:

Nishijima Y and Juodkazis S (2015)
*Optical characterization and lasing in
three-dimensional opal-structures.*
Front. Mater. 2:49.
doi: 10.3389/fmats.2015.00049

The lasing properties of dye-permeated opal pyramidal structures are compared with the lasing properties of opal films. The opal-structures studied were made by sedimentation of microspheres and by sol-gel inversion of the direct-opals. Forced-sedimentation by centrifugation inside wet-etched pyramidal pits on silicon surfaces was used to improve the structural quality of the direct-opal structures. Single crystalline pyramids with the base length of $\sim 100\ \mu\text{m}$ were formed by centrifuged sedimentation. The lasing of dyes in the well-ordered crystalline and poly-crystalline structures showed a distinct multi-modal spectrum. Gain via a distributed feedback was responsible for the lasing since the photonic band gap was negligible in a low refractive index contrast medium; the indices of silica and ethylene glycol are 1.46 and 1.42, respectively. A disordered lasing spectrum was observed from opal films with structural defects and multi-domain regions. The three-dimensional structural quality of the structures was assessed by *in situ* optical diffraction and confocal fluorescence. A correlation between the lasing spectrum and the three-dimensional structural quality was established. Lasing threshold of a sulforhodamine dye in a silica opal was controlled via Förster mechanism by addition of a donor rhodamine 6G dye. The lasing spectrum had a well-ordered modal structure, which was spectrally stable at different excitation powers. The sharp lasing threshold characterized by a spontaneous emission coupling ratio, $\beta \simeq 10^{-2}$, was obtained.

Keywords: colloidal crystals, opals, lasing, micro-fabrication, Förster energy transfer, microscopy, diffraction

1. Introduction

Photonic crystals (PhCs) (John, 1987; Yablonovitch, 1987) fabricated by top-down or bottom-up methods are being used for a growing number of applications, such as spontaneous emission control (Li et al., 2007), micro lasing (Matsubara et al., 2008; Nishijima et al., 2008), and refractive index sensing (Nishijima et al., 2007; Kita et al., 2008; Wu et al., 2008). PhCs can also be combined with plasmonics to yield new methods for controlling photo-excited processes, which for example, can result in an enhancement of fluorescence (Tawa et al., 2008). Opals are a class of PhCs, which could potentially be used for many applications, because opal structures covering macroscopically large areas can be easily fabricated by self-assembly of (sub-)micrometer sized spheres. Opal and inverse-opal structures with a well-controlled three-dimensional (3D) morphology could find various uses relating to PhCs, micro lasers, structured waveguides, and magneto-optical applications (Conti and Fratallocchi, 2008; Choueikani et al., 2009).

One of the problems associated with the fabrication of large opal structures is the difficulty to control the crystalline quality of the face-centered-cubic opals even when the microspheres used for sedimentation have a small, ~1%, size distribution. It was recently demonstrated that a narrow, ~1%, size distribution of microspheres is essential for obtaining high-fidelity photonic stopgaps and wave guiding in Si-inverse opals (Lavrinenko et al., 2009). Developing methods for controlling the structure of the opal sedimentation lattices and selecting between face-centered-cubic (fcc) and hexagonal-closest-packing (hcp) symmetry is a key area of research concerning the growth of artificial opals (Velasco et al., 1998; Auer and Frenkel, 2001). The fcc and hcp packings have nearly equal Helmholtz formation energies (Bolhuis et al., 1997; Bruce et al., 1997; Pronk and Frenkel, 1999, 2003). Therefore, in order to control the colloidal crystal morphology, colloid epitaxy (Santamaria et al., 2002), deposition on a micro patterned surface by sedimentation (Mizeikis et al., 2001), or dip-coating using Langmuir–Blodgett technique (Hur and Won, 2008) are used. Recently, a spatially constrained deposition using a pyramidal template fabricated in silicon by anisotropic etching was proposed for the formation of well-defined opals (Matsuo et al., 2003).

Another problem of opal and inverse-opal fabrication is that self-assembly often results in the formation of poly-crystalline domains. This is caused by a concentration of the colloidal suspension during evaporation, which facilitates multi-site nucleation (Biben et al., 1993). Opals with a poly-crystalline structure are not useful for photonic applications where single crystal order is required. Films of opals sedimented on substrates with pins dry-etched on the surface resulted in monocrystal opals (Mizeikis et al., 2001). However, the pins only imposed the order on three to five adjacent mono layers depending on the size of the microspheres.

The sedimentation process used for forming the opals can also affect their quality. Slow gravitational sedimentation and formation of opals at low evaporation rates are not practical since they are lengthy process and require efficient suppression of mechanical vibrations. Furthermore, the possibility of stacking faults is not negligible when these techniques are used. This is because the high colloidal concentration can lead to multi-site nucleation (Hoogenboom et al., 2002). Sedimentation of opals in 2 and 3D constrained micro volumes could prospectively solve the problems mentioned above because constrained micro volumes impose the order onto the structure.

Transport of electrons and energy in photo-excited molecular systems is in focus of basic and applied research due to prospects to unveil functioning of photosynthesis (Ben-Shem et al., 2003). Different linear and non-linear (Kamada et al., 2007; Hirakawa et al., 2008) optical microscopy methods are used to measure the energy transfer in micro-cavities (Fujiwara et al., 2005) and living cells (Sasaki et al., 1991; Hotta et al., 2006). The principles of photo-excitation and interaction of materials at atomic and molecular level in artificially engineered three-dimensional (3D) structures, such as photonic crystals (PhCs) (John, 1987; Yablonovitch, 1987), high-Q, and random and distributed feed back (DFB) cavities (Wright et al., 2004), are currently under active investigation due to prospects of miniaturization of opto-electronic devices, solar batteries, and creation of alternative light sources.

The 3D confinement of photo-excited materials and control of their (de-)excitation by external cavity or via spatial localization of light–matter interaction has prospects to advance photonics into new multi-disciplinary fields. Better understanding of these processes might lead toward miniaturization of opto-electronic devices.

Here, we demonstrate the formation of well-ordered opals by sedimentation in wet-etched micro-pits in silicon by fast centrifugation (Nishijima, 2009), which the single crystalline fcc opal photonic crystals with large area and short time can be obtained. The resulting three-dimensional structures were characterized by confocal fluorescence and optical diffraction and compared with opal-structures obtained on flat substrates. Lasing of dye-soaked opals showed a well-ordered multi-mode spectrum, and a correlation between the structural quality and lasing spectrum was established. Rhodamine 6G (Rh6G) and sulforhodamine 101 (SRh) were used for the energy transfer studies inside silica opals. These dyes are suitable for a fluorescent and resonance energy transfer system; they have a high fluorescence quantum yield (~1%), similar chemical structures (similar ground state and excited-state dipole momenta), and a high overlap of energy donor (Rh6G) fluorescence and acceptor (SRh) absorption spectra. The lasing properties of these dyes inside opal photonic structures show potential application in fluidic micro-laser field.

2. Experimental

2.1. Fabrication and Characterization of Opal Structures

Single crystal opals were fabricated using an Si template-assisted method (Matsuo et al., 2003). Opal structures were made by centrifuged sedimentation of SiO₂ spheres (diameter 300 nm) at 5,000 rpm for 10 min on a cover glass substrates ~1-mm-thick (Nishijima et al., 2007). After centrifuge, the opal structures were dried and annealed at 500°C/5 h for drying and sintering into a mechanically stable film. Structures were lifted from the pits by adhesive peeling off. Opal films were made by centrifuge sedimentation onto flat glass under the same conditions. The structural quality was inspected by scanning electron microscopy (SEM). The surface of the structure was a (111) face plane of the face-centered-cubic (fcc) structure.

The template had pyramidal pits anisotropically etched along the <111> direction on a (100) surface of Si, covered by 1 μm layer of oxide. The pattern of pits was realized by lithography using a positive photo resist OFPR5000 (Tokyo Ohka Kogyo Co. Ltd.). Following exposure and development of the photoresist, the pattern was dry-etched into the oxide layer using a gas mixture of SF₆ and C₄F₈. The patterned oxide was then used as a mask for wet etching of the silicon using a KOH aqueous solution (33 wt%, with 1 wt% isopropanol). Etching accompanied by sonication was carried out for 4 h, and pyramidal pits were obtained.

Inversion of both the films and pyramids was performed using a sol-gel process. The polystyrene opals were immersed into a tetraethoxysilane (TEOS) sol, which was prepared from TEOS, ethanol, and HCl (at 1:1:0.1 ratio in volume fraction) mixture. The residual polystyrene was removed from the structures by washing in ethyl acetate.

The structural quality was inspected by scanning electron microscopy (SEM). The surface of the structure was a (111) face plane of the face-centered-cubic (fcc) structure.

2.2. Lasing in Opal Structures

The laser dyes were rhodamine 6G (Rh6G, from Wako Pure chemical industries, Ltd.) and sulforhodamine 101 (SRh, from Exciton, Inc.). The molar extinction coefficient of the dyes at the laser excitation wavelength of 532 nm was 99,000 and 23,800 $M^{-1} \text{ cm}^{-1}$ for Rh6G and SRh, respectively.

The emission spectra of dye-soaked opal films were measured by micro-spectroscopic setup consisting of microscope (IX-71, Olympus) equipped with an objective lens of 40 \times magnification and numerical aperture of $NA = 0.55$, and spectrometer (SpectraPro, Acton) with liquid nitrogen-cooled CCD camera. The excitation source was a Nd:YAG laser emitting 7 ns duration pulses at 532 nm (Indi, Spectra Physics) with the repetition rate of 10 Hz. Low repetition rate was allowed to avoid thermal accumulation.

3. Results and Discussion

Figure 1 shows a scanning electron microscopy (SEM) image of a pit on an Si template, a silica opal formed from 300-nm-diameter microspheres, and an inverse-opal obtained via sol-gel inversion from polystyrene opals. Thermal sintering of opals inside the template caused partial adhesion of the microspheres to the template. After peeling the pyramids off, the adhesion caused some defects to the surface. When sol-gel inversion was implemented to make silica pyramids, the side-wall quality was even better (**Figure 1C**). When the same sedimentation conditions were used on cover glass substrates, poly-crystalline opal films with a thickness of up to 100 μm were formed with the typical single crystalline domains having a cross-section of 10–30 μm (as judged by a SEM observation from a single surface layer).

3.1. Optical Characterization of Opals

3.1.1. Confocal Fluorescence Imaging

Since SEM observation does not provide information on the internal 3D structural quality, we applied confocal optical imaging and

diffraction to obtain information of the 3D structure as described below. The relation between the structural 3D ordering and the lasing from the same regions was then investigated.

The internal structure of the opals was carried out by confocal imaging of fluorescence from a dye solution, which was pipette-dropped onto the opal-structures and allowed to permeate them. The soaked structures were then placed on the stage of an Olympus microscope equipped with an FV-300 scanning system, and imaged. a cw-HeNe laser at 543 nm wavelength was used for illumination (principle scheme of characterization setup is shown in **Figure 2**). The beam was scanned across the sample using galvanometer-mirrors. Focusing was carried out with a 100 \times magnification oil-immersion objective lens of numerical aperture $NA = 1.30$. Fluorescence of the rhodamine B dye in an ethylene glycol solution ($1.0 \times 10^{-5} \text{ M}$) in the opal structure was detected by a photo-multiplier tube through a confocal pinhole of a 60 μm diameter. The optical setup is shown in **Figure 2A**. The confocal fluorescence imaging was limited to structures comprising microspheres with a diameter of 1 μm or larger. This is because of the optical spatial resolution $\sim \lambda$ of the confocal microscope. Also, the imaging was limited to the small sized pyramids, because of the working distance of the objective lens and the inhibition of scattering from particles. In the past, it has been shown that optical diffraction can be used to assess the 3D internal order of opals (Kanai et al., 2005; Santamaria et al., 2005; Lopez, 2006). Therefore, we used this technique to characterize structures made of smaller particles and larger pyramids.

The optical diffraction pattern represents a Fourier transform of the crystal structure (**Figure 2B**). Lopez et al. demonstrated that the optical conditions necessary to obtain the diffraction patterns are given by Santamaria et al. (2002) and Lopez (2006):

$$\frac{a}{\lambda} \geq m \frac{\sqrt{2}}{n} \left[1 + \frac{(2s-1)}{3} \right]^{\frac{1}{2}}, \quad (1)$$

where a is the lattice constant (424 nm in our case), s and m are two integers, which represent the set of diffraction spots and the diffraction order, respectively. The lowest energy light quanta that satisfy this condition are $\frac{a}{\lambda} = \frac{1.633}{n}$ ($m = s = 1$) and the next possible diffraction pattern is defined by $\frac{a}{\lambda} = \frac{2.828}{n}$ ($m = 1, s = 2$).

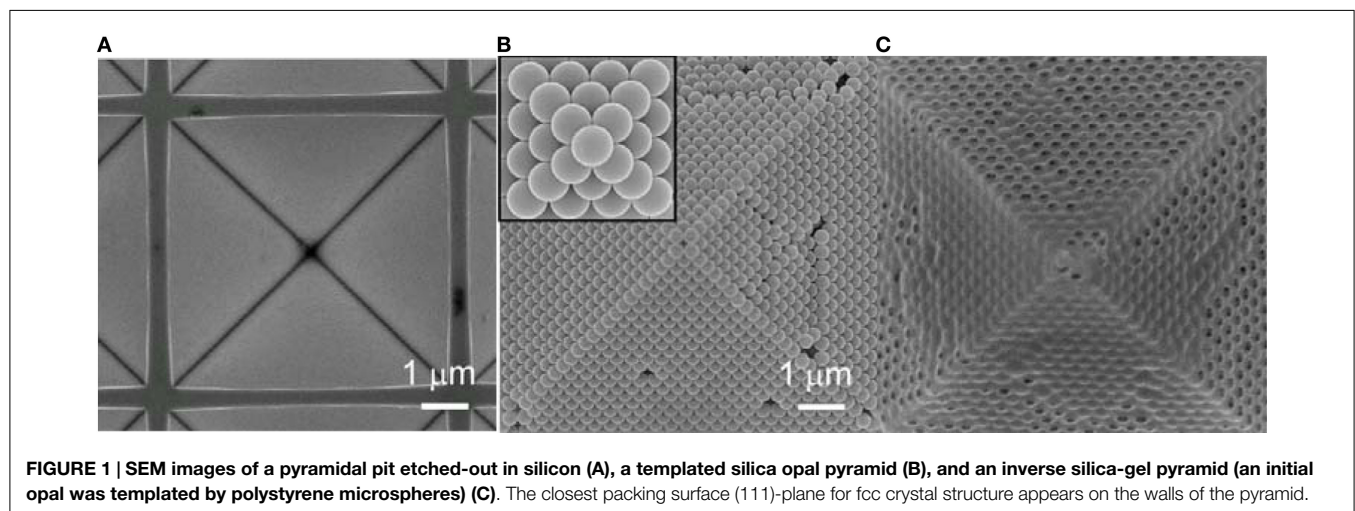
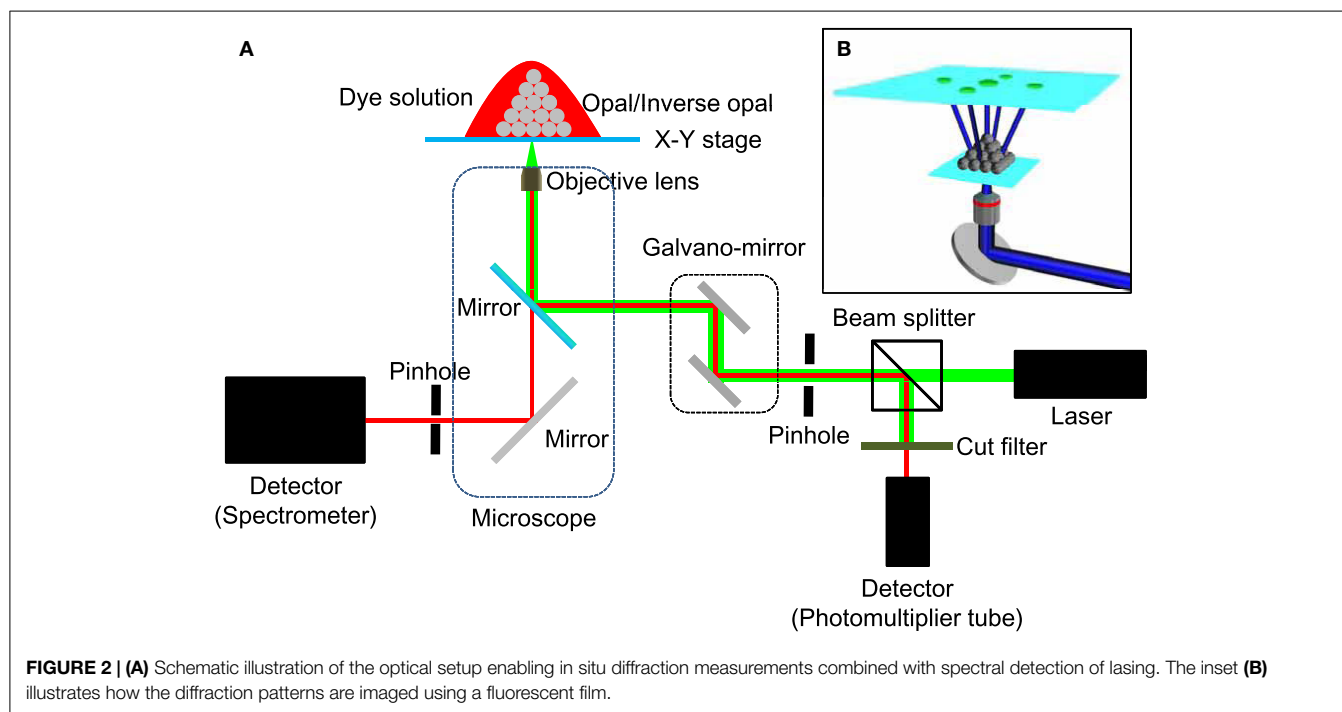


FIGURE 1 | SEM images of a pyramidal pit etched-out in silicon (A), a templated silica opal pyramid (B), and an inverse silica-gel pyramid (an initial opal was templated by polystyrene microspheres) (C). The closest packing surface (111)-plane for fcc crystal structure appears on the walls of the pyramid.



In our case, $\frac{a}{\lambda} = 1.18$ and only the lowest energy diffraction pattern can appear. The optical diffraction, or the Fourier transform of three-dimensional crystal structures, was compared with fast Fourier transform (FFT) images of two-dimensional SEM data of the opal surfaces.

In order to test the quality of our structures using diffraction, we used the setup shown in **Figure 2**. The pulses of a femtosecond laser at 360 nm wavelength (82 MHz, 150 fs, the second harmonics of a Tsunami laser, Spectra Physics) were focused on to the bottom side of the samples using a $4\times$ NA = 0.13 objective lens. The diffracted beams were projected on to a coumarine 6-doped thin polystyrene film, and the fluorescence image was collected by a CCD camera.

Laser emission from the structures was also measured. In order to obtain lasing, the samples were soaked in the solution of rhodamine B and ethylene glycol used for confocal imaging. These structures were then pumped with a frequency-doubled Nd:YAG nanosecond laser operating at a wavelength of 532 nm, a repetition frequency of 10 Hz, and with a pulse duration of ~ 7 ns. The laser beam was coupled into an inverted microscope and focused on the sample using either an objective lenses of $40\times$ magnification and a numerical aperture NA = 0.55 or an objective with $10\times$ magnification and a numerical aperture NA = 0.25. The sample was mounted on a translation stage attached to the microscope and oriented with the bases of the pyramids [or the (111) crystallographic planes of the opal structure] normal to the optical axis of the objective lens. Emission from the rhodamine B ethylene glycol solution (5.0×10^{-4} M) was detected by imaging the surface of the sample (base plane of the pyramids) via the same objective lens used for focusing the pump beam. The collected radiation was analyzed using a spectrometer with 1200 groves/mm grating (resolution < 0.1 nm) with a liquid nitrogen-cooled CCD detector (**Figure 2A**).

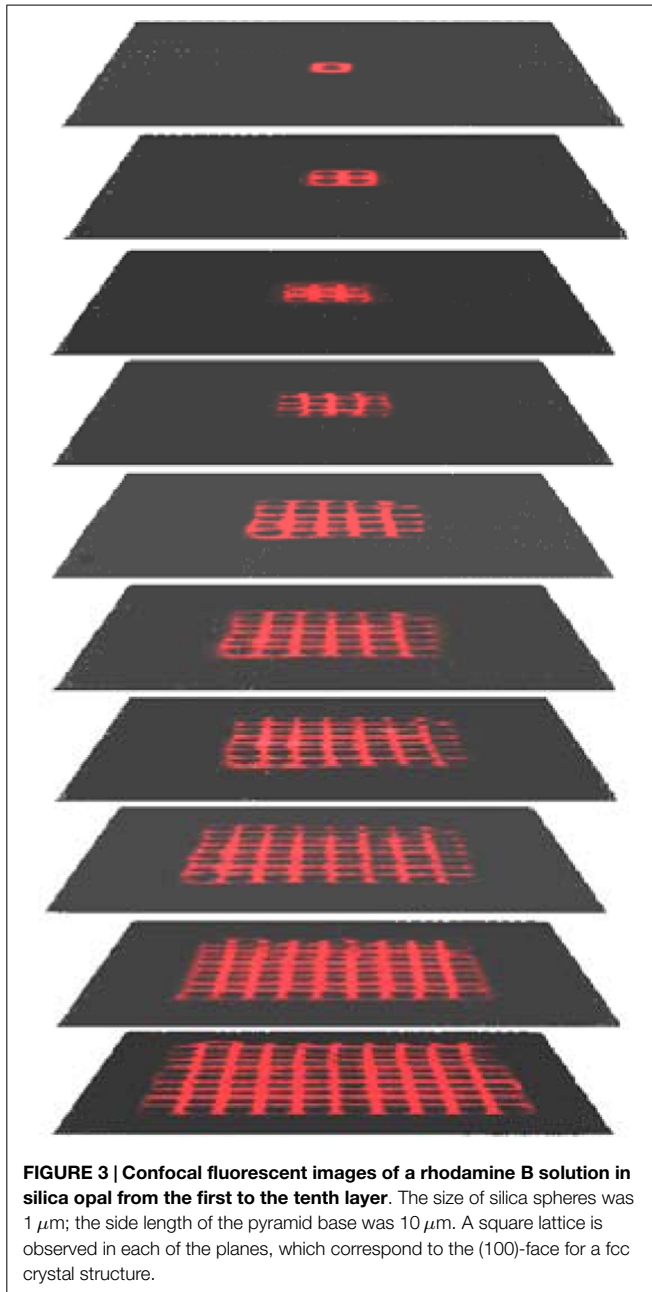
In order to study the connection between the 3D structural quality of the opals and their lasing properties, optical diffraction and lasing were measured on the same areas using the setup shown in **Figure 2**. First, the optical diffraction was measured on the chosen region/structure. Then, the structure was soaked in dye, and the lasing spectrum was measured. Prior to the optical measurements, the same areas were inspected by SEM. There was an offset of about $10 \mu\text{m}$ between the areas measured by SEM and the areas upon which the optical measurements were performed. This offset occurred because the SEM measurements and the optical characterization were carried out with different setups.

Figure 3 shows the fluorescence from an opal structure. The similarity in the refractive indices of silica ($n = 1.46$) and ethylene glycol (1.42) reduced light scattering and facilitated reliable imaging of several layers.

Confocal imaging of the structures showed that the odd and even layers have the same alternating order (**Figure 3**), indicating that the particles formed an fcc structure with the pyramid base being a (100) plane of the fcc structure.

3.1.2. Optical Diffraction

Figure 4 shows the optical diffraction patterns from pyramids of different sizes. The diffraction patterns from larger structures show more scattering. Nevertheless, the fcc structure can be recognized in the diffraction patterns. The presented analysis shows that optical diffraction can be implemented *in situ* (as opposed to *ex situ* SEM analysis) and can be used to assess the structural quality of regions, which were subsequently used for lasing. SEM images of several regions in $10 \mu\text{m}$ -thick opal films, along with their Fourier transform and the measured diffraction patterns are shown in **Figure 5**. The Fourier transform of the SEM images (column 2) reveal that hexagonal diffraction pattern from a close packing surfaces along $<111>$ direction of opal films are expected.



The most ordered regions with just a few point defects (vacancies) show orderly diffraction patterns. The diffraction from less ordered regions near the grain boundaries shows two superimposed and $\pi/6$ -rotated patterns. The $\pi/6$ rotational misalignment is the maximum possible between the two neighboring domains in a $\langle 111 \rangle$ plane. Finally, the regions with a large number of grains and smaller than 10 periods in cross-section showed a typical disordered amorphous pattern of Fourier image. These 2D-FFT patterns are consistent with the optical diffraction images (column 3), which reveal a 3D order of the samples.

3.2. Lasing Pyramidal Opals

Figure 6 shows the lasing emission spectrum of rhodamine B dye solution in the poly-crystalline opal film. The lasing threshold

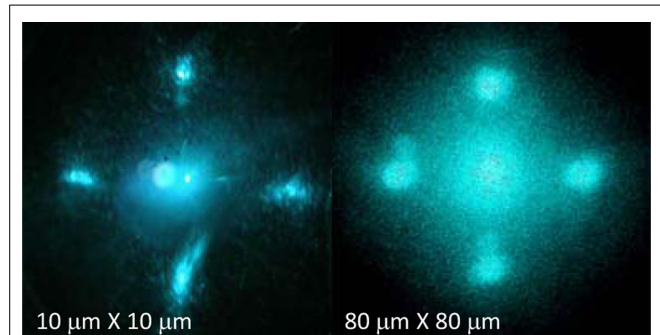


FIGURE 4 | Optical diffraction of pyramidal opals of different sizes. The diameter of the silica microspheres was $300\ \text{nm}$; illumination wavelength $360\ \text{nm}$. Laser beam was directed along to the $\langle 100 \rangle$ direction to the fcc crystal lattice (perpendicular to the base of a pyramid).

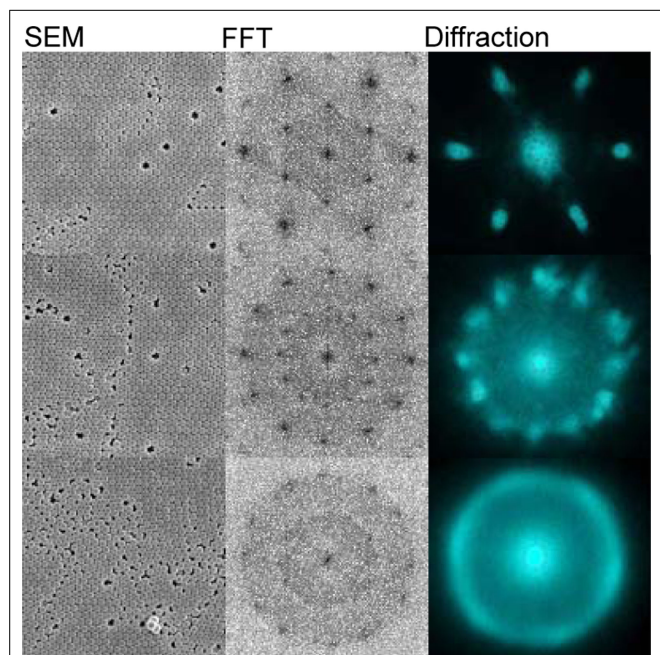
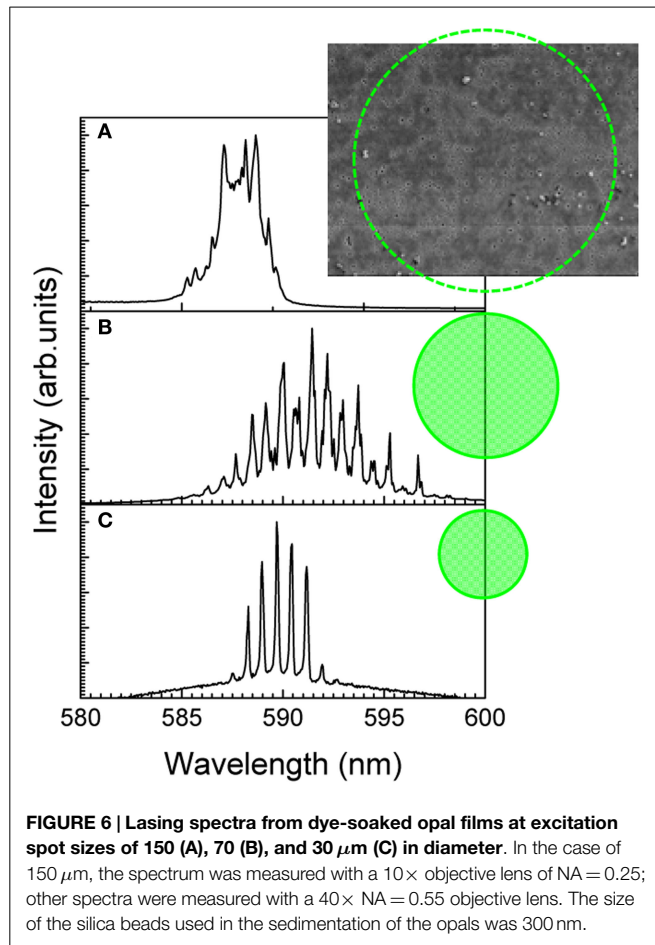


FIGURE 5 | SEM images and their 2D-FFT together with the optical diffraction (Figure 2B) from three typical regions in the opal films. The crystalline order of the regions decreases from top to bottom of the figure. The optical diffraction and SEM were not taken from exactly the same areas and can be compared only qualitatively. The diameter of the silica microspheres was $300\ \text{nm}$ and the illumination wavelength was $360\ \text{nm}$. The structure was illuminated along the $\langle 111 \rangle$ direction of the opal films (perpendicular to the film).

was determined from the power dependence of the emission when the spectrum became spectrally structured. At pump powers above the lasing threshold, the mode intensity increased exponentially with excitation while the spectral intensity outside of the modes decreased. The spectra shown in **Figure 6** were taken at approximately 10% above the lasing threshold.

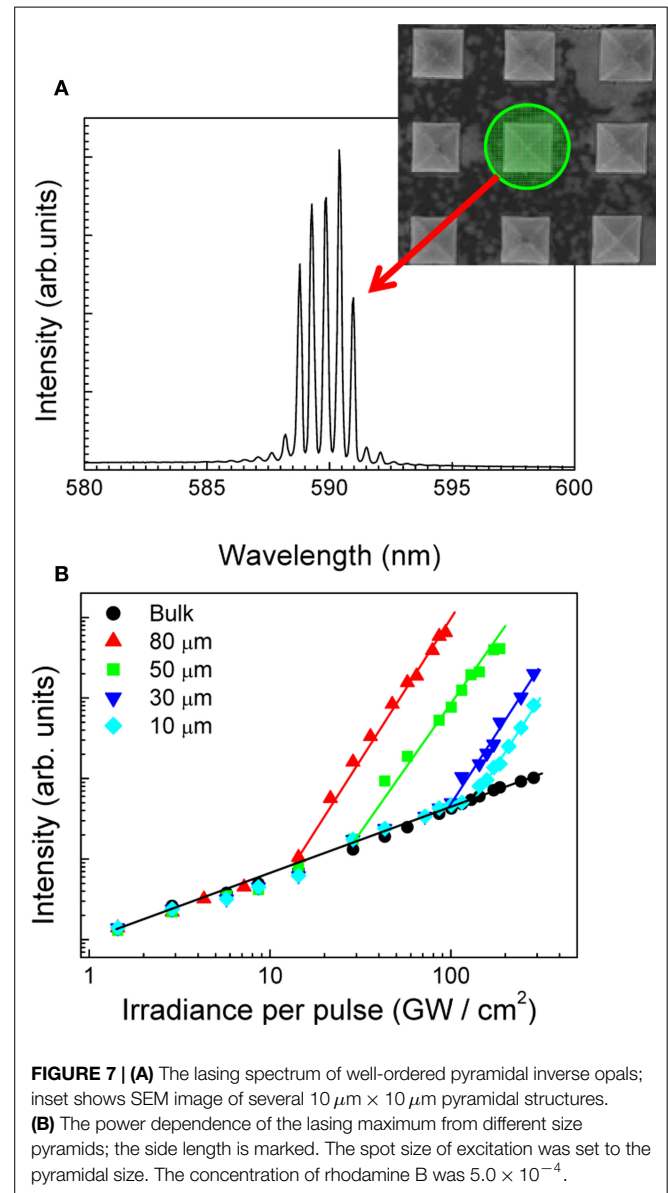
When the excitation area was larger than $\varphi > 150\ \mu\text{m}$ in diameter (**Figure 6A**), the spectra were disordered similar to that previously reported from random structures (Frolov et al., 1999; Shkunov et al., 2001). The optical diffraction patterns from such



regions were amorphous as well (Figure 5). In the case of 70 μm areas, more regular spectra were obtained, although there was still some sub-structure and small peaks. The typical optical diffraction from such regions showed a distinct few domain structure (as shown in the middle pattern in Figure 5). Well-ordered spectra with regular sharp and periodic peaks were obtained when the spot size was 70 μm and approximately corresponded to a single crystalline domain as observed by the optical diffraction. The lasing peaks were separated by 0.77 nm interval. Similar well-ordered lasing was observed from the inverse opals (Figure 7A).

The inverse-opal structures could prospectively be used for gain amplification since the volume fraction of the immersed dye is approximately three times larger than that in direct-opals.

Figure 7A shows the lasing spectrum of a dye-soaked pyramidal single crystal inverse-opal. We measured 10 different regions on the film (as shown in Figure 6C) and 10 different pyramids, which showed single crystalline patterns of optical diffraction. The lasing modes of all structures and regions tested had the same spectral positions to within ± 0.3 nm for the opal films and ± 0.15 nm for the pyramidal single crystal. This corroborates that the single pyramidal crystals have better wavelength stability of the lasing modes. This type of lasing is not defined by the photonic band gap because of the low refractive index contrast between silica (1.46) and ethylene glycol (1.42) (Kitamura et al., 2007; Nishijima, 2009; Nishijima et al., 2009a). Rather, it is determined



by the distributed feedback (DFB) in the dye as demonstrated recently (Nishijima et al., 2008). The lasing threshold and the onset of lasing were determined from the power dependence of the lasing spectrum shown in Figure 7B.

Further studies are necessary to model and experimentally verify the directionality of the lasing modes. In this study, the directionality of excitation and laser emission were integrated due to comparatively tight focusing. The influence of a micro-sphere size distribution on the lasing spectrum predicted recently (Gottardo et al., 2008) should also be investigated.

The emission spectra of dye-soaked opal films were measured by micro-spectroscopic setup consisting of microscope (IX-71, Olympus) equipped with an objective lens of 40 \times magnification and numerical aperture of NA = 0.55, and spectrometer (SpectraPro, Acton) with liquid nitrogen-cooled CCD camera. The excitation source was a Nd:YAG laser emitting 7 ns duration

pulses at 532 nm (Indi, Spectra Physics) with the repetition rate of 10 Hz. Low repetition rate allowed to avoid thermal accumulation.

Figure 8 shows normalized absorption and fluorescence spectra of the dyes Rh6G and SRh. The marked dashed region shows an overlap of absorption-emission bands of the pair in a 500–650 nm wavelength region. The dyes permeated silica opal film, which was templated using a 300 nm diameter silica microspheres. The concentration of the acceptor dye (SRh) was 1.0 mM, and the donor dye concentration was varied (0, 0.8, 1.4, 1.8, 2.0 mM). **Figure 9** shows the absorption spectra of the each dye solution measured in a 100 μm optical path.

3.3. Förster Energy Transfer

Interaction between two lasing dyes in opal structures is discussed next. The Förster theory of dipole–dipole energy transfer (Forster, 1947, 1948, 1959) defines the efficiency of a radiative

excitation state energy transfer in a donor–acceptor system, which is dependent on the separation r and is expressed as (Birks, 1970):

$$k_{ET}(r) = \frac{(9000 \ln 10) \kappa^2}{128 \pi^5 n^4 N_A r^6 T_D} \int_0^\infty \frac{F_D(\tilde{\nu}) \varepsilon_A(\tilde{\nu})}{\tilde{\nu}^4} d\tilde{\nu} \quad (2)$$

$$= \frac{1}{r^6} \left(\frac{R_0}{r} \right)^6$$

where F_D is the fluorescence spectral profile of the donor species, ε_A is the molar extinction coefficient of the acceptor molecule; R_0 is the critical transfer distance, which depends on the donor oscillator strength and spectral overlap, κ is the orientation factor ($\kappa^2 = 2/3$ in the case of a random directional distribution), N_A is the Avogadro number, $\tilde{\nu}$ is the wave number, T_D is the excited-state lifetime of the energy donor (Rh6G in our study), n is the refractive index (ethylene glycol ~ 1.42).

Equation (2) indicates that a spectrally overlapping absorption–emission of the donor–acceptor pairs is prospective for the efficient energy transfer via a Förster mechanism. Studies of energy transfer in combinations of pyrene–perylene, two different coumarin dyes, and fluorescein–ethidium bromide, have been carried out with applications in biological imaging and bio-analytical science (Takakusa et al., 2003; Fujiwara et al., 2005; de Almeida et al., 2007; Stevens et al., 2009). Overlap of the fluorescence and absorption was estimated from our experiments as $6.9 \times 10^{-15} \text{ mol}^{-1} \text{ cm}^6$ (**Figure 8**), and the critical Förster radius was calculated as 3.1 nm.

Figure 8 shows normalized absorption and fluorescence spectra of the dyes Rh6G and SRh. The marked dashed region shows an overlap of absorption-emission bands of the pair in a 500–650 nm wavelength region. The dyes permeated silica opal film which was templated using a 300 nm diameter silica microspheres. The concentration of the acceptor dye (SRh) was 1.0 mM, and the donor dye concentration was varied (0, 0.8, 1.4, 1.8, 2.0 mM). Absorption spectra of the each dye solution measured in a 100 μm optical path in shown in **Figure 9**.

Lasing experiments of dye-soaked opal films from the defect-free regions with cross-section of $\sim 20 \mu\text{m}$ were chosen for excitation-emission measurements. **Figure 10** shows the lasing spectra of dye solutions in the opal film. The Rh6G solution (without SRh) spectra showed lasing with a well-ordered modal structure. The lasing mechanism is due to a gain distributed feedback (DFB) since the refractive index contrast between the silica and dye solution was negligible, and there were no formation of photonic stop gap (Nishijima et al., 2009a). With the addition of SRh (into Rh6G), the lasing of Rh6G changed into amplified spontaneous emission (ASE) while lasing of SRh at the longer wavelength was obtained. The modal structure of the lasing SRh emission was similar to that observed in pure Rh6G.

Lasing requires a population inversion of excited-state dye molecules within their excitation lifetimes which are ~ 4 and 5 ns for Rh6G and SRh, respectively. The excitation pulse duration of 7 ns was longer than the luminescence lifetime and limits the population inversion (Magde et al., 1999). Inhibition of the R6G lasing clearly indicates an energy transfer between Rh6G and SRh. The pair of dyes becomes a Förster donor–acceptor pair or, in terms of lasing in a four-level system, the donor absorption ($1 \rightarrow 2$ transition) feeds the emission ($3 \rightarrow 4$). The decay rates of SRh are: radiative, $k_r = 2.0 \times 10^8 \text{ s}^{-1}$, and non-radiative,

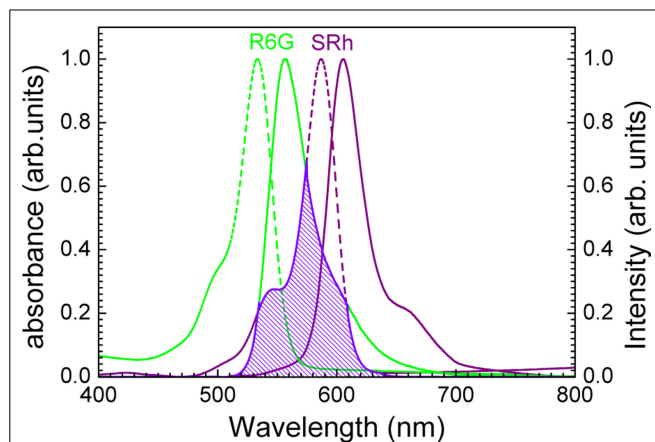


FIGURE 8 | Absorption (dashed lines) and fluorescence (solid lines) spectra of Rh6G and SRh. The donor–acceptor overlap used for calculation of the Förster radius is highlighted.

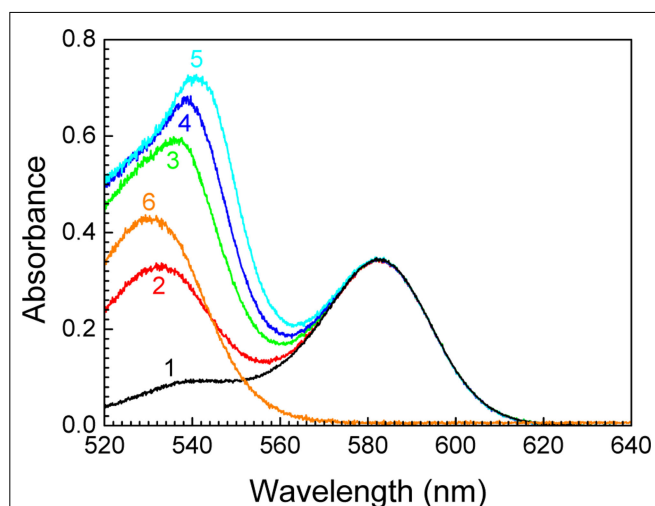


FIGURE 9 | Absorption spectra of dye mixtures: 1 mM of SRh with Rh6G at concentrations 0 (1), 0.8 (2), 1.4 (3), 1.8 (4), 2.0 mM (5) in ethylene glycol; absorption of 1 mM solution of Rh6G is given by curve (6). Sample thickness was 70 μm .

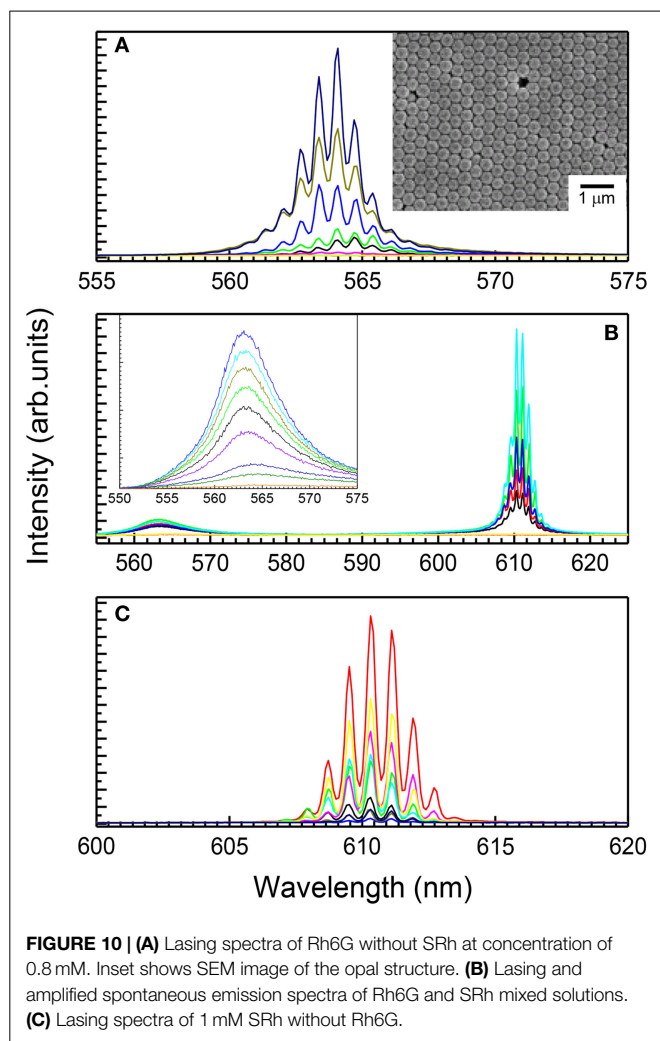


FIGURE 10 | (A) Lasing spectra of Rh6G without SRh at concentration of 0.8 mM. Inset shows SEM image of the opal structure. **(B)** Lasing and amplified spontaneous emission spectra of Rh6G and SRh mixed solutions. **(C)** Lasing spectra of 1 mM SRh without Rh6G.

$k_{nr} = 8.6 \times 10^7 \text{ s}^{-1}$. The energy transfer $2 \rightarrow 3$ takes place at the rate $k_{ET}(r) = 2.2 \times 10^{-43} r^{-6}$. Before decaying (within 5 ns), the excited SRh molecules should form a donor–acceptor pair with separation $< 3 \text{ nm}$.

Figure 11 summarizes data on lasing intensity vs. excitation irradiance. Before lasing, the emission increases linearly on excitation (slope 1 in a log–log presentation). At the lasing threshold, a non-linear increase of intensity was observed. A gain saturation was reached at high irradiance with the onset of linear dependence. Interestingly, the lasing threshold and slope of the non-linear part depended on the concentration of donor dye. The lasing threshold of SRh increased with addition of Rh6G as well as the slope of non-linear part. This demonstrates an inhibition of direct excitation of SRh by a 532 nm excitation laser light with increasing concentration of Rh6G, which is a strong absorber (**Figure 9**). Without Rh6G, the non-linear slope was 1.83 and changes to 2.21 (2), 2.45 (3), 3.34 (4), and 6.30 (5) with increased concentrations of Rh6G. This increase of slopes indicates that effective excitation state formation and population inversion of SRh was achieved due to energy transfer.

The other interesting point of this lasing phenomenon is that the gain-saturated point of lasing is almost the same for each concentration of dye solution. The efficiency of excited-state

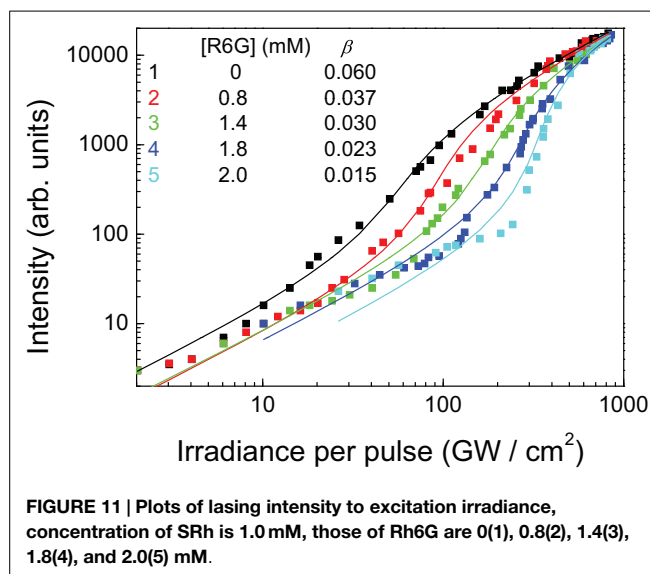


FIGURE 11 | Plots of lasing intensity to excitation irradiance, concentration of SRh is 1.0 mM, those of Rh6G are 0(1), 0.8(2), 1.4(3), 1.8(4), and 2.0(5) mM.

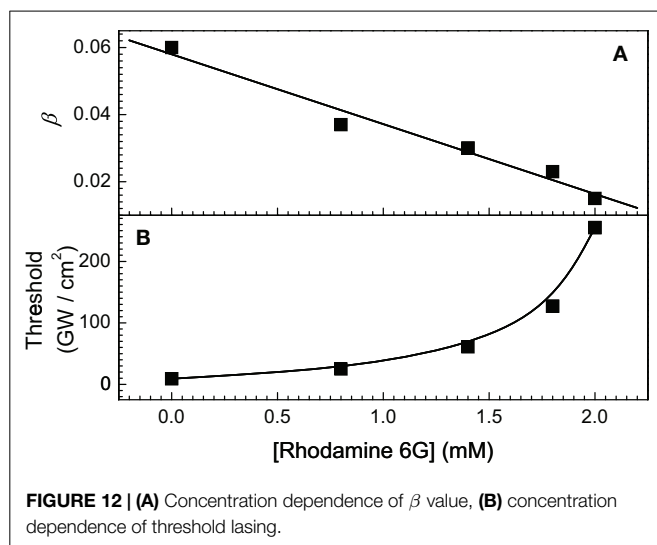
energy transfer between Rh6G and SRh is high and is demonstrated in a 3D structure, the opal film. Weak fluorescence of Rh6G still remained, since the energy transfer efficiency is not 100%.

The dependence of a lasing threshold on donor–acceptor concentrations can be quantified via a spontaneous emission coupling ratio β (Horowicz et al., 1992; Takashima et al., 2008). To determine the β value, defined as the fraction of spontaneous emission coupled into a lasing mode with respect to the spontaneous emission into all modes, the input–output power relationship was modeled using a rate equation (Yokoyama and Brorson, 1989; Kippenberg et al., 2006):

$$s = \frac{-1}{2\beta} + \frac{p}{2\Omega} + \frac{\sqrt{(\beta p - \Omega)^2 + 4p\beta^2\Omega}}{2\Omega\beta}, \quad (3)$$

where s is the cavity photon number (proportional to the emission intensity), p is the pump rate (of emitting species), and Ω is the cavity loss rate. This equation was used to fit experimental data with changeable parameters Ω and β . The Ω values were typically 4.0 ± 1 and were not correlated with β .

The best fit β values at different concentration of donor molecules (Rh6G) are plotted in **Figure 12**. With an increasing concentration of Rh6G, β value was decreasing with a well-expressed threshold-like switch-on lasing behavior. In the mixed solution of R6G (energy donor) and SRh (energy acceptor), lasing from Rh6G has never been observed at the used pump powers. This can be explained by an efficient energy transfer via Förster mechanism when, during the life time of the excited donor of approximately few nanoseconds, the energy transfer to the acceptor dye occurred more efficiently and a population inversion of R6G had never occurred. The lowest energy level, the fluorescence band of SRh, was lasing in this system of dye mixture. The lasing threshold increased with increasing concentration of absorbing Rh6G. The non-linear slope of the log–log plot of power dependence can be explained by energy transfer from Rh6G to SRh, which assisted the population inversion of the latter. With an increasing concentration of donor, the probability of energy transfer was also increasing. The small $\beta \sim 10^{-2}$ value represents



a strongly non-linear threshold-like switch-on mechanism of lasing, which could find applications in sensor and opto-fluidic applications.

4. Conclusion

We showed that pyramidal templates enable fabrication of single crystalline opal structures. This is because the templates reduce the number of free-surfaces, which always make a destabilizing contribution in structure formation. Hence, by reducing free surfaces (using a template), it is possible to generate well-ordered structures in far-from-equilibrium conditions. Centrifugation helps to facilitate the formation of single crystalline structure in pyramids since destabilizing factors, such as Brownian motion and mechanical vibrations, which plague equilibrium sedimentation, become negligible.

We showed a correlation between the lasing spectrum and the structural quality of opal-structures in both direct and inverse-opal films and pyramidal structures. Single crystalline regions of opal-structures showed well-ordered multi-modal lasing spectra, while poly-crystalline structures showed a less ordered lasing spectra. In both cases, the spectral separation of

modes is defined by the gain-DFB (Nishijima et al., 2009a). Structural 3D characterization of the opals can be carried out using the same setup, which is used to measure photoluminescence and lasing, thereby enabling the correlation between opal structure and its lasing properties to be determined. Establishing the connections between the structural and surface quality of 3D complex structures and their optical functions is required in number of fields in photonics and sensing.

Lasing of a donor-acceptor pair dyes with the presence of strong Förster energy transfer is demonstrated inside silica opals. The Förster energy transfer in a higher refractive index contrast 3D photonic structures with photonic stop gap could further enhance the energy transfer when the donor emission is forbidden by the stop gap and a single-mode lasing is realized (Nishijima et al., 2008). The spectral positions of the lasing modes were stable at the all range of employed laser pumping powers. The lasing mechanism was the gain-DFB. Miniaturized DFB lasers using opal structures as well as micro lasers based on evanescent wave amplification around a colloidal micro-sphere (Datsyuk et al., 2005a,b) are promising directions for miniaturized optically pumped lasers. Such micro-opal patterns can be easily integrated into microfluidic environment (Misawa and Juodkazis, 1999; Juodkazis et al., 2008) providing new functionalities in sensors and laser tweezer applications.

Author Contributions

YN contributed to the concept of the work, designed and carried our experiments, prepared the first draft. SJ contributed to the concept of structural characterization and two dyes lasing, analyzed data, and edited the manuscript.

Acknowledgments

This work is based on the Ph.D. theses of YN. We thank Professor Hiroaki Misawa for continuous support and encouragement during these studies. We are grateful to Professors Shigeki Matsuo, Vitaly Datsyuk, and Sajeev John for discussions. *Funding:* SJ is grateful for the support by ARC Discovery DP130101205 grant.

References

- Auer, S., and Frenkel, D. (2001). Prediction of absolute crystal-nucleation rate in hard-sphere colloids. *Nature* 409, 1020–1023. doi:10.1038/35059035
- Ben-Shem, A., Frolow, E., and Nelson, N. (2003). Crystal structure of plant photosystem I. *Nature* 426, 630–635. doi:10.1038/nature02200
- Biben, T., Hansen, J. P., and Barrat, J. L. (1993). Density profiles of concentrated colloidal suspensions in sedimentation equilibrium. *J. Chem. Phys.* 98, 7330–7344. doi:10.1063/1.464726
- Birks, J. B. (1970). *Photophysics of Aromatic Molecules*. London: Wiley-Interscience.
- Bolhuis, P. G., Frenkel, D., Mau, S.-C., and Huse, D. A. (1997). Entropy difference between crystal phases. *Nature* 388, 235. doi:10.1038/40779
- Bruce, A. D., Wilding, N. B., and Ackland, G. J. (1997). Free energy of crystalline solids: a lattice-switch Monte Carlo method. *Phys. Rev. Lett.* 79, 3002–3005. doi:10.1103/PhysRevLett.79.3002
- Choueikani, F., Royer, F., Jamon, D., Siblini, A., Rousseau, J. J., Neveu, S., et al. (2009). Magneto-optical waveguides made of cobalt ferrite nanoparticles embedded in silica/Zirconia organic-inorganic matrix. *Appl. Phys. Lett.* 94, 051113. doi:10.1063/1.3079094
- Conti, C., and Fratallocchi, A. (2008). Dynamic light diffusion, three-dimensional Anderson localization and lasing in inverted opals. *Nat. Phys.* 4, 794–798. doi:10.1038/nphys1035
- Datsyuk, V. V., Juodkazis, S., and Misawa, H. (2005a). Comparison of the classical and quantum rates of spontaneous light emission in a cavity. *Phys. Rev. A* 72, 025803. doi:10.1103/PhysRevA.72.025803
- Datsyuk, V. V., Juodkazis, S., and Misawa, H. (2005b). Properties of a laser based on evanescent-wave amplification. *J. Opt. Soc. Am. B* 22, 1471–1478. doi:10.1364/JOSAB.22.001471
- de Almeida, R. F. M., Borst, J., Fedorov, A., Manuel Prieto, Z., and Visser, A. J. W. G. (2007). Complexity of lipid domains and rafts in giant unilamellar vesicles revealed by combining imaging and microscopic and macroscopic time-resolved fluorescence. *Biophys. J.* 93, 539–553. doi:10.1529/biophysj.106.098822
- Forster, T. (1947). Experimental and theoretical investigation of intermolecular transfer of electron activation energy. *Z. Naturforsch.* 4a, 321–327.
- Forster, T. (1948). Zwischenmolekulare energiewanderung und fluoreszenz. *Ann. Physik.* 437, 55. doi:10.1002/andp.19484370105
- Forster, T. (1959). 10th spiers memorial lecture transfer mechanism of electronic excitation. *Discuss. Faraday. Soc.* 27, 7–17. doi:10.1039/d19592700007

- Frolov, S., Vardeny, Z., Zakhidov, A., and Baughman, R. (1999). Laser-like emission in opal photonic crystals. *Opt. Commun.* 162, 241–246. doi:10.1016/S0030-4018(99)00089-9
- Fujiwara, H., Sasaki, K., and Masuhara, H. (2005). Enhancement of Forster energy transfer within a microspherical cavity. *Chemphyschem* 6, 2410–2416. doi:10.1002/cphc.200500318
- Gottardo, S., Sapienza, R., García, P. D., Blanco, A., Wiersma, D. S., and López, C. (2008). Resonance-driven random lasing. *Nat. Phot.* 2, 383–446. doi:10.1038/nphoton.2008.102
- Hirakawa, S., Kawamata, J., Suzuki, Y., Tani, S., Murafuji, T., Kasatani, K., et al. (2008). Two-photon absorption properties of azulanyl compounds having a conjugated ketone backbone. *J. Phys. Chem. A* 112, 5198–5207. doi:10.1021/jp800415b
- Hoogenboom, J. P., Derks, D., Vergeer, P., and Blaaderen, A. (2002). Stacking faults in colloidal crystals grown by sedimentation. *J. Chem. Phys.* 117, 11320–11328. doi:10.1063/1.1522397
- Horowitz, R. J., Heitmann, H., Kadota, Y., and Yamamoto, Y. (1992). Gaas micro-cavity quantum-well laser with enhanced coupling of spontaneous emission to the lasing mode. *Appl. Phys. Lett.* 61, 392–394. doi:10.1063/1.107893
- Hotta, J., Ujii, H., and Hofkens, J. (2006). The fabrication of a thin, circular polymer film based phase shaper for generating doughnut modes. *Opt. Express* 14, 6273–6278. doi:10.1364/OE.14.006273
- Hur, J., and Won, Y.-Y. (2008). Fabrication of high-quality non-close-packed 2d colloid crystals by template-guided Langmuir-Blodgett particle deposition. *Soft Matter* 4, 1261–1269. doi:10.1039/b716218a
- John, S. (1987). Strong localization of photons in certain disordered dielectric superlattices. *Phys. Rev. Lett.* 58, 2486–2489. doi:10.1103/PhysRevLett.58.2486
- Juodkazis, S., Mizeikis, V., Matsuo, S., Ueno, K., and Misawa, H. (2008). Three-dimensional micro- and nano-structuring of materials by tightly focused laser radiation. *Bull. Chem. Soc. Jpn.* 81, 411–448. doi:10.1246/bcsj.81.411
- Kamada, K., Antonov, L., Yamada, S., Ohta, K., Yoshikawa, T., Tahara, K., et al. (2007). Two-photon absorption properties of dehydrobenzo[12]annulenes and hexakis(phenylethynyl)benzenes: effect of edge-linkage. *Chemphyschem* 8, 2671–2677. doi:10.1002/cphc.200700555
- Kanai, T., Sawada, T., and Kitamura, K. (2005). Air-pulse-drive fabrication of photonic crystal films of colloids with high spectral quality. *Adv. Funct. Mater.* 15, 25–29. doi:10.1002/adfm.200305160
- Kippenberg, T. J., Kalkman, J., Polman, A., and Vahala, K. J. (2006). Demonstration of an erbium-doped micro-disk laser on a silicon chip. *Phys. Rev. A* 74, 051803(R). doi:10.1103/PhysRevA.74.051802
- Kita, S., Kengo, N., and Baba, T. (2008). Refractive index sensing utilizing a cw photonic crystal nanolaser and its array configuration. *Opt. Express* 16, 8174–8180. doi:10.1364/OE.16.008174
- Kitamura, N., Fukumi, K., Nishii, J., and Ohno, N. (2007). Relationship between refractive index and density of synthetic silica glasses. *J. Appl. Phys.* 101, 123533. doi:10.1063/1.2748861
- Lavrinenko, A. V., Wohlleben, W., and Leyrer, R. J. (2009). Influence of imperfections on the photonic insulating and guiding properties of finite Si inverted opal crystals. *Opt. Express* 17, 747–760. doi:10.1364/OE.17.000747
- Li, J., Jia, B., Zhou, G., Bullen, C., Serbin, J., and Gu, M. (2007). Spectral redistribution in spontaneous emission from quantum-dot-infiltrated 3d woodpile photonic crystals for telecommunications. *Adv. Mater.* 19, 3276–3280. doi:10.1002/adma.200602054
- Lopez, C. (2006). Three-dimensional photonic bandgap materials: semiconductors for light. *J. Opt. A* 8, R1–R14. doi:10.1088/1464-4258/8/5/R01
- Magde, D., Rojas, G. E., and Seybold, P. G. (1999). Solvent dependence of the fluorescence lifetimes of xanthene dyes. *Photochem. Photobiol.* 70, 737–744. doi:10.1111/j.1751-1097.1999.tb08277.x
- Matsubara, H., Yoshimoto, S., Saito, H., Yue, J. L., Tanaka, Y., and Noda, S. (2008). Gan photonic-crystal surface-emitting laser at blue-violet wavelengths. *Science* 319, 445–447. doi:10.1126/science.1150413
- Matsuo, S., Fujine, T., Fukuda, K., Juodkazis, S., and Misawa, H. (2003). Formation of free-standing micro-pyramid colloidal crystals grown on silicon substrate. *Appl. Phys. Lett.* 82, 4283–4285. doi:10.1063/1.1583138
- Misawa, H., and Juodkazis, S. (1999). Photophysics and photochemistry of a laser manipulated microparticle. *Prog. Polym. Sci.* 24, 665–697. doi:10.1016/S0079-6700(99)00009-X
- Mizeikis, V., Juodkazis, S., Marcinkevicius, A., Matsuo, S., and Misawa, H. (2001). Tailoring and characterization of photonic crystals. *J. Photochem. Photobiol. C* 2, 35–69. doi:10.1021/ar700143w
- Nishijima, Y. (2009). *Spectroscopic Studies of Opal and Inverse Opal Photonic Crystals*. Ph.D. thesis, Hokkaido University, Sapporo
- Nishijima, Y., Ueno, K., Juodkazis, S., Mizeikis, V., Fujiwara, H., and Misawa, H. (2009a). Lasing with well-defined cavity modes in dye-infiltrated silica inverse opals. *Opt. Express* 17, 2976–2983. doi:10.1364/OE.17.002976
- Nishijima, Y., Ueno, K., Juodkazis, S., Mizeikis, V., Misawa, H., Maeda, M., et al. (2008). Tunable single-mode photonic lasing from zirconia inverse opal photonic crystals. *Opt. Express* 16, 13676. doi:10.1364/OE.16.013676
- Nishijima, Y., Ueno, K., Juodkazis, S., Mizeikis, V., Misawa, H., Tanimura, H., et al. (2007). Inverse silica opal photonic crystals for optical sensing applications. *Opt. Express* 15, 12979–12988. doi:10.1364/OE.15.012979
- Pronk, S., and Frenkel, D. (1999). Can stacking faults in hard-sphere crystals anneal out spontaneously? *J. Chem. Phys.* 110, 4589–4592. doi:10.1063/1.478339
- Pronk, S., and Frenkel, D. (2003). Large difference in the elastic properties of fcc and hcp hard-sphere crystals. *Phys. Rev. Lett.* 90, 255501. doi:10.1103/PhysRevLett.90.255501
- Santamaria, F. G., Galisteo-Lopez, J. F., Braun, P. V., and Lopez, C. (2005). Optical diffraction and high-energy features in three-dimensional photonic crystals. *Phys. Rev. B* 71, 195112. doi:10.1103/PhysRevB.71.195112
- Santamaria, F. G., Miyazaki, H. T., Urquia, A., Ibisate, M., Belmonte, M., Shinya, N., et al. (2002). Nanorobotic manipulation of microspheres for on-chip diamond architectures. *Adv. Mater.* 14, 1144–1147. doi:10.1002/1521-4095(20020816)14:16<1144::AID-ADMA1144>3.0.CO;2-I
- Sasaki, K., Koshioka, M., and Masuhara, H. (1991). Tree-dimensional space- and time resolved fluorescence spectroscopy. *Appl. Spectroscopy* 45, 1041. doi:10.1366/0003702914336336
- Shkunov, M. N., DeLong, M. C., Raikh, M. E., Vardeny, Z. V., Zakhidov, A. A., and Baughman, R. H. (2001). Photonic versus random lasing in opal single crystals. *Synth. Met.* 116, 485–491. doi:10.1016/S0379-6779(00)00420-3
- Stevens, N., O'Connor, N., Vishwasrao, H., Samaroo, D., Kandel, E. R., Akins, D. L., et al. (2009). Two color RNA intercalating probe for cell imaging applications. *J. Am. Chem. Soc.* 130, 7182–7183. doi:10.1021/ja800892a
- Takakusa, H., Kikuchi, K., Urano, Y., and Tetsuo Nagano, H. K. (2003). A novel design method of ratiometric fluorescent probes based on fluorescence resonance energy transfer switching by spectral overlap integral. *Chem. Eur. J.* 9, 1479–1485. doi:10.1002/chem.200390167
- Takahashi, H., Fujiwara, H., Takeuchi, S., Sasaki, K., and Takahashi, M. (2008). Control of spontaneous emission coupling factor β in fiber-coupled microsphere resonators. *Appl. Phys. Lett.* 92, 071115. doi:10.1063/1.2884329
- Tawa, K., Hori, H., Kintaka, K., Kiyosue, K., Tatsu, Y., and Nishii, J. (2008). Optical microscopic observation of fluorescence enhanced by grating-coupled surface plasmon resonance. *Opt. Express* 16, 9781–9789. doi:10.1364/OE.16.009781
- Velasco, E., Mederos, L., and Navascus, G. (1998). Phase diagram of colloidal systems. *Langmuir* 14, 5652–5655. doi:10.1021/la980126y
- Wright, D., Brasselet, E., Zyss, J., Langer, G., and Kern, W. (2004). Dte-doped organic distributed-feedback lasers with index and surface gratings: the role of pump polarization and molecular orientation. *J. Opt. Soc. Am. B* 21, 944–950. doi:10.1364/JOSAB.21.000944
- Wu, J., Day, D., and Gu, M. (2008). A microfluidic refractive index sensor based on an integrated three-dimensional photonic crystal. *Appl. Phys. Lett.* 92, 071108. doi:10.1063/1.2840700
- Yablonoivitch, E. (1987). Inhibited spontaneous emission in solid-state physics and electronics. *Phys. Rev. Lett.* 58, 2059–2062. doi:10.1103/PhysRevLett.58.2059
- Yokoyama, H., and Brorson, S. D. (1989). Rate equation analysis of microcavity lasers. *J. Appl. Phys.* 66, 4801–4805. doi:10.1364/OE.18.009909

Conflict of Interest Statement: The authors declare that the research was conducted in the absence of any commercial or financial relationships that could be construed as a potential conflict of interest.

Copyright © 2015 Nishijima and Juodkazis. This is an open-access article distributed under the terms of the Creative Commons Attribution License (CC BY). The use, distribution or reproduction in other forums is permitted, provided the original author(s) or licensor are credited and that the original publication in this journal is cited, in accordance with accepted academic practice. No use, distribution or reproduction is permitted which does not comply with these terms.